Pure Appl. Chem., Vol. 77, No. 2, pp. 475–485, 2005.
DOI: 10.1351/pac200577020475

Thermal plasma deposition from thick to thin coatings and from micro- to nanostructure*

P. Fauchais‡, M. Vardelle, J. F. Coudert, A. Vardelle, C. Delbos, and J. Fazilleau

SPCTS-UMR 6638 CNRS, University of Limoges, France

Abstract: This paper is devoted to the presentation of our actual knowledge in plasma spraying. It presents successively: the parameters controlling the impact of the molten particles onto the substrate and resulting splat formation followed by splats layering and coating formation; the engineering of nano- or finely structured coatings with different possible routes; and the actual possibilities for the on-line control of the spray process.

Keywords: plasma spraying; suspension plasma spraying; plasma torches; particle flattening; splats; coating formation.

INTRODUCTION

Plasma spraying is part of thermal spraying processes in which finely divided metallic and nonmetallic materials are deposited in a molten or semi-molten state on a prepared substrate [1]. The base material/coating combination can be tailored to provide resistance to heat, wear, erosion, and/or corrosion, as well as unique sets of surface characteristics. Coatings are also used to restore worn or poorly machined parts to original dimensions and specifications. In conventional plasma spraying, more than 97 % of coatings are manufactured with direct current (dc) arcs, and less than 3 % with radio frequency (rf) discharges [2]. Plasmas are mainly used to spray refractory materials, superalloys, and more generally high-added-value materials either in air or controlled atmosphere. Typical coating thickness ranges between 50 μm and a few millimeters. At impact onto the substrate, the molten particles flatten and form lamellae (splats) which layering forms the coating. Splats have columnar or equiaxed structures with grain sizes between 50 and 200 nm. However, this fine structure is altered by grain size effect and large volume fraction of internal interfaces [3].

During the last three decades, many efforts have been devoted to a better understanding of the mass, momentum, and heat transfer between plasma and particles in order to adapt plasma working conditions and particle size and morphology to the desired impact velocities and temperatures [2]. This was achieved thanks to measuring devices [4], making it possible to back models [5]. Such measurements have allowed the development, during the last decade, of simplified on-line control, or, more precisely, monitoring systems that are now used in industrial spray booths [6]. During this last decade, numerous studies were devoted to splat formation [7], but none to coating formation. Finally, during recent years, different techniques were tested for engineering nano- or finely structured coatings [8].

In this paper, we present our actual knowledge of the splat and coating formation, engineering of nano- or finely structured coatings, optimization of the spray torches, and particle injection to achieve such coatings with possible on-line control of the deposition process.

---

*Paper based on a presentation at the 16th International Symposium on Plasma Chemistry (ISPC-16), Taormina, Italy, 22–27 June 2003. Other presentations are published in this issue, pp. 345–495.

‡Corresponding author

CONVENTIONAL PLASMA-SPRAYED COATINGS

General remarks

There are two main routes to manufacture plasma-sprayed coatings:

- The first route consists in spraying particles in a solid or plastic state at velocities high enough to get plastic deformation upon impact followed by impact consolidation. This is achieved, for example, with the cold spray technique [9] with impact velocities v_p higher than 700 m/s for particles with diameter d_p below 20 μm. Dense coatings of ductile materials (Cu, Al, …) exempt from the oxidation formed during the spray process, can be achieved. Such technologies are still in their infancy.
- At the moment, plasma torches working close to atmospheric pressure cannot accelerate particles over 700 m/s (generally $40 < v_p < 400$ m/s [2]). Therefore, only fully or partially melted particles can be sprayed. The splats are formed by the flattening and solidification of the molten drops. Generally, the next droplet impacts on an already-solidified splat. The reaction of the molten particles with environment is promoted, especially when a convection movement is induced within the drop by the plasma flow [10].

For plasma-sprayed particles, droplet flattening and splat layering are very complex and, besides the flux of impacting particle ($\approx 10^7$/s), involve various time and length scales as shown in Table 1.

Table 1 Various time and length scales characteristic of the spray process .

Length range	Particle flattening and cooling	Time between two successive impacts	Pass or layer formation	Time between two passages of the torch
From splats (μm) to parts to be sprayed (up to meters)	<10 μs	10–100 μs	Few ms	Few s to few h

Splat formation

Figure 1 summarizes the parameters that control the splat formation.

The parameters at impact are often described through dimensionless numbers [11] that depend strongly on the particle impact velocity v_p and temperature T_p. The latter controls the particle specific mass $\rho_p(T_p)$, its viscosity $\mu_P(T_p)$, and surface tension $\sigma_P(T_p)$. The main numbers used are the Reynolds number ($Re = \rho_{p*} v_{P*} d_P/\mu_P$) that characterizes the viscous dissipation of inertia forces, Weber number ($We = \rho_{p*} v_P{}^2{}_* d_P/\sigma_P$) that is the ratio of impact energy to surface energy, and Mach number ($M_a = v_P/a_P$ where a_P is the sound velocity in the liquid). For example, with a liquid steel droplet ($a_P \approx 3000$ m/s) impacting at 300 m/s, M_a is about 0.1, and the compressibility effects can be neglected. With such velocities, the impact pressure is about 7.10^9 Pa, but it is released over 3.10^{-10} s, very short time com-

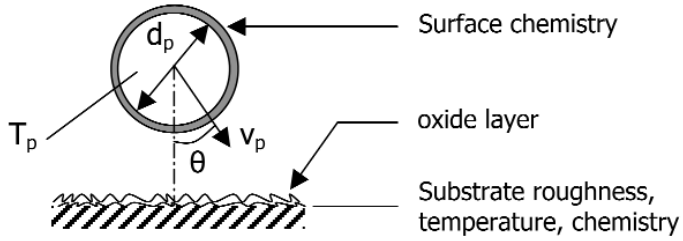

Fig. 1 Parameters controlling splat formation.

pared to the droplet flattening time (≈1 μs). However, the most difficult point is to determine the effect of the particle surface chemistry, substrate oxide layer, and roughness on particle flattening, the latter parameters modifying the particle wettability.

Impact splashing

For water, ethanol, and gasoline droplets impacting on smooth substrates (Ra < 0.1 μm), the Sommerfeld number ($K = We^{0.5}Re^{0.25}$) determines the particle behavior at impact: $K < 3$ corresponds to the rebound of the impacting particle, $3 < K < 58$ to deposition and $K > 58$ to splashing [12]. Under plasma conditions, K ranges between 10 and 2000. Escure et al. [12], using a fast camera (50 ns) triggered by the light signals used to measure v_P and d_P (phase doppler anemometry) and T_P (50-ns two-color pyrometry) prior to particle impact (2 mm over the substrate) have shown that, taking into account the measurement acuracy, the limit of splashing is also close to 58. Figure 2 shows the deposition and splashing of alumina particles. It is worth noting that for $d_P \approx 30$ μm, the splashed droplets are in the 0.1–1 μm range and that they reach a distance of about 3 mm above the substrate outside the flow boundary layer. It means that most of them are most likely entrained by the hot gas flow close to the substrate. Of course, as soon as the substrate roughness increases, splashing also occurs for K values below 58. Recent measurements of Cedelle et al. [13] have shown that the impact splashing of a 30-μm particle occurs about 100 ns after its impact. Assuming a sound velocity of about 3000 m/s within the liquid, 100 ns correspond to the propagation of the wave from the bottom to the top of the droplet. This impact splashing is quite different from the flattening splashing occurring at the end of the flattening process, i.e., in the μs time range and described in the next section.

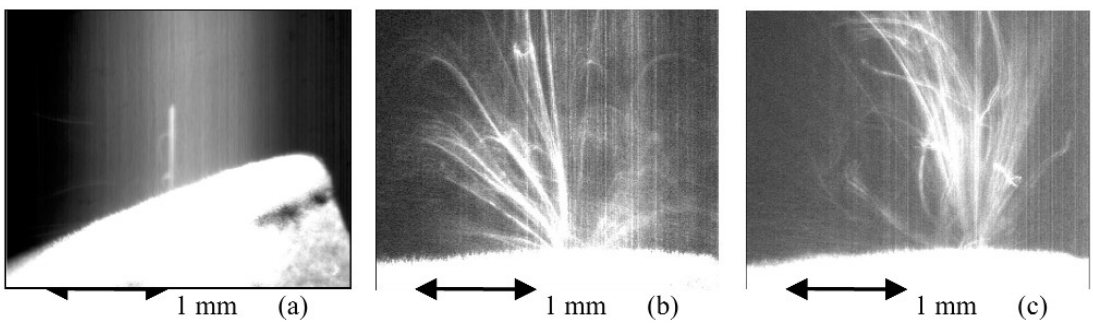

Fig. 2 Impact splashing for different Sommerfeld parameters (alumina particles): (a) deposition $K = 30$; (b) splashing $K = 229$; and (c) splashing $K = 858$.

Flattening splashing

At the end of the flattening process, and depending on the fact that solidification starts before flattening is completed or not, splats may either be extensively fingered or disk-shaped as shown for zirconia splats in Fig. 3. As summarized in a review paper [7], the cooling rates and diameter evolution of the flattening particles have been measured at the University of Limoges (M. Vardelle et al. [14–16]) and CNRC (C. Moreau et al. [17–19]). The flattening evolution has also been measured for mm-sized particles exhibiting the same Reynolds and Peclet numbers as plasma-sprayed particles, at Toyohashi University (J. M. Fukumoto et al. [20]) and Toronto University (N. Z. Mehdizadeh et al. [21]). The experimental observations have shown that a transition temperature T_t exists depending on the surface chemistry of the particle at impact and substrate material and surface oxidation (oxide layer thickness and composition). When the substrate is preheated below T_t, splats are extensively fingered (flattening

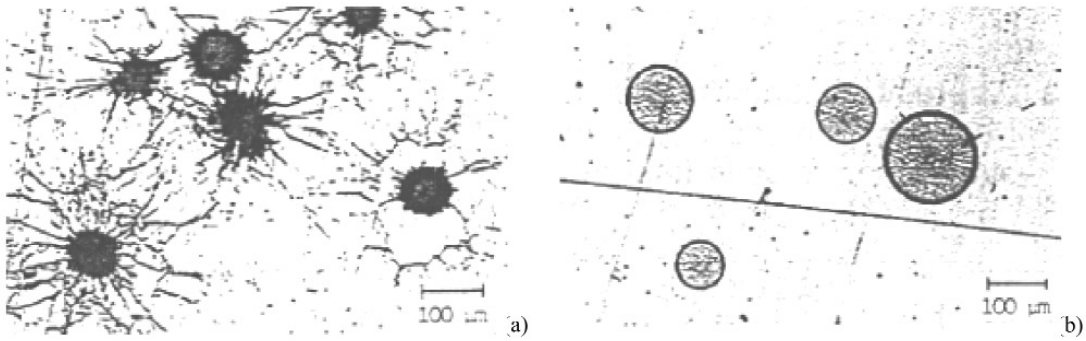

Fig. 3 Zirconia splats deposited on polished stainless steel 304L substrate (a) extensively fingered $T_s < 500$ K, (b) disk-shaped $T_s > 500$ K.

splashing parallel to the substrate), while over T_t they are disk-shaped. The quality of contact between the substrate and splat depends on substrate preheating temperature T_s relatively to T_t.

If $T_s > T_t$, the contact between splat and substrate is excellent, except in the splat rim, while if $T_s < T_t$, the interface structure is porous. In the first case, the grain size within the splat is 2 to 4 times smaller than in the second case. This is confirmed by the cooling rate CR measurements. For zirconia particles sprayed on 304L stainless steel substrates when $T_s > T_t$ (≈500 K), $10^8 < CR < 10^9$ K/s, while when $T_s < T_t$, $10^7 < CR < 10^8$ K/s. This difference in cooling rates can be linked to the thermal contact resistance R_{th} between the splat and substrate. For $T_s > T_t$, $R_{th} < 10^{-7}$ m^2·K/W, while for $T_s < T_t$, $R_{th} > 10^{-6}$ m^2·K/W, which in fact corresponds to smaller contact area between splat and substrate.

The parameters that affect T_t are not yet quite clear, but the most sound explanations [7] are the following:

- The desorption of adsorbates and condensates.
- A better wetting between the splat and substrate. Wetting increases with substrate roughness (at least for Ra < 100 nm) and depends on the surface chemistry: For example when, spraying metals on metals, the oxide layer formed at the surface of the in-flight droplet and the oxide layer at the substrate surface will affect splat formation. In-flight oxidation is linked to the spray conditions and substrate oxidation, to the way it has been preheated: preheating time t s, preheating temperature T_s, and preheating rate dT_s/dt. These last parameters condition the oxide thickness, composition, and roughness. It explains why the most sophisticated models such as those developed by the team of Mostaghimi at Toronto: 3D flow on rough substrates, cooling and solidification of the flattening particle taking into account R_{th} and wettability, flattening-splashing based on the Rayleigh–Taylor instability theory [22] are not always in agreement with experiments.

It has to be emphasized that increasing the roughness increases splashing but much less when $T_s > T_t$. The splat adhesion also decreases as soon as the impact angle θ (see Fig. 1) is over 30–45° depending on the sprayed material.

Influence of impact parameters

The ratio of the splat diameter D to the impacting particle diameter d_p, according to the different theories [7], varies as Re^{α}, with for most of them $\alpha = 0.2$. Thus, for given values of T_p over the melting temperature and particle diameter d_p, D increases with v_p and correlatively the splat thickness decreases. As the latter decreases, the particle cooling rate increases resulting in finer grains or columns within splats [23–25]. Typical values of grain sizes are between 50 and 200 nm. It is also important to limit the values of T_p over the melting temperature because when it increases too much, particle evaporation in flight is promoted [26].

Coating formation

Thermomechanical properties of coatings depend first on splat flattening and second on their cooling and layering with a huge time range [24]: (see Table 1). The mean temperature T_c toward which the coating tends after a few hundreds of ms also varies slowly with time according to the torch passages [7]. The splat layering and temperature evolution between T_p and T_c and, then, between T_c and room temperature control the coating residual stresses: quenching, expansion mismatch, mean temperature T_c fluctuation, impact (if $v_p > 300$–400 m/s), and their relaxation mechanisms: cracks, creep, yielding, interfacial sliding [27,28].

The value of the mean coating temperature T_c (generally higher than that of the substrate T_s) relative to the transition temperature T_t is also very important. Over T_t, the contacts between splats and substrate are improved correspondingly increasing the quenching stress. The adhesion/cohesion of coatings, generally sprayed on rough substrates, is increased by a factor of 2 to 4 when T_s and T_c are over $T_{t.}$

The models of coating formation [29] rely on statistical models (Monte Carlo methods…) with given particle temperature, velocity, and size distributions at impact. Assumptions are made on splat formation and curling. However, the splats layering, taking into account the substrate or previously deposited layer roughness, impact angle as well as residual stresses with their relaxation mechanisms is far to be representative of the reality, and such models are still in their infancy. When particles are overheated, the vapor resulting from evaporation, eventually after its reaction with the surrounding atmosphere (oxidation, for example) may be condensed in the plasma jet fringes and deposited between successive passes creating defects [30] especially when the surface temperature is high (over 700–800 K), which eases their sticking.

NANO- OR FINELY STRUCTURED COATINGS

Even if the splat microstructures are fine (column or grain sizes between 50–200 nm), they are altered by grain size effects and large volume fractions of internal interfaces. In plasma spray process, which generally consists in melting the particles, it is, thus, a challenge to keep a fine- or nanostructure.

The following four routes are possible.

Spraying agglomerates of nanoparticles

Particles are made of nanosized grains (<200–500 nm). The trick upon spraying is to melt only the external shell of the particles [31] or to have agglomerates of different melting points (Al_2O_3 and TiO_2) [3,32], see Fig. 4. It results in coatings containing areas of agglomerated unmelted nanoparticles. Their mechanical properties exhibit a bi-modal distribution. Of course, high-impact velocities ($v_p > 300$ m/s) are required to densify the nanostructured parts and, thus, improve coating wear resistance.

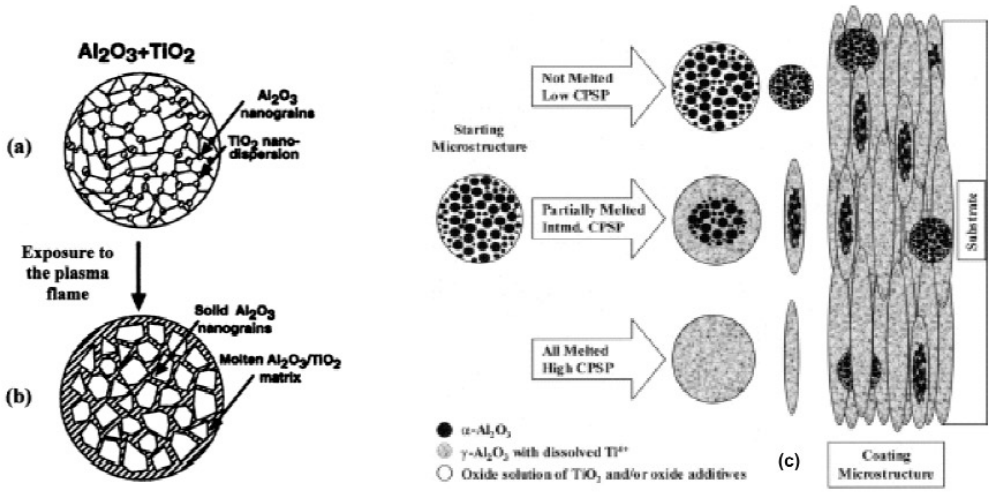

Fig. 4 Schematic of (a) an Al_2O_3–TiO_2 granule [3], (b) the partly melted granule where solid Al_2O_3 nanograins exist within the liquid TiO_2 [3], and (c) the resulting coating [32].

Metallic glasses

Steel particles with numerous compounds and a hyper-cooling temperature smaller than that of glass transition are plasma sprayed, and splats cooled rapidly. The resulting metallic glass has a low density of defects such as tiny cracks and holes. The super-hard steel coating is then heated to create a structure made up of crystal grains from 2–75 nm. The coating hardness is similar to best tungsten carbide coatings [33].

Injection of liquid precursors

Very different types of liquid precursors have been injected in flames or plasma jets: nitrates, isopropoxides, butoxides… dissolved in isopropanol; n-butanol. The liquid is evaporated, and liquid or solid nanoparticles are synthesized [34]. However, coatings are more or less powdered and must be densified, for example, by sintering, to the expense of grain growth.

Injection of suspensions

A suspension of nanoparticles (50–300 nm agglomerates) is injected in dc plasma jets in order to produce liquid droplets below 5 μm. The liquid is evaporated in less than 1 μs, and the melted agglomerates are sprayed as molten particles with diameters at impact between 0.1–1 μm [35]. It results in splats with diameter ranging between 0.2–3 μm and thickness between 20–80 nm (Fig. 5). They can be deposited at a rate of 10 $\mu m/m^2 \cdot h$ (about 3–5 times less than conventional spraying, but one order of magnitude more than CVD coatings). The coating thickness can vary between 1 μm and hundreds of μm. The deposition process is similar to that of conventional spraying with a drastic influence of the preheating temperature relatively to transition temperature. The resulting coatings can be either rather dense (Fig. 6) with porosities in the hundreds of nm range or rather porous ($P > 20$ %).

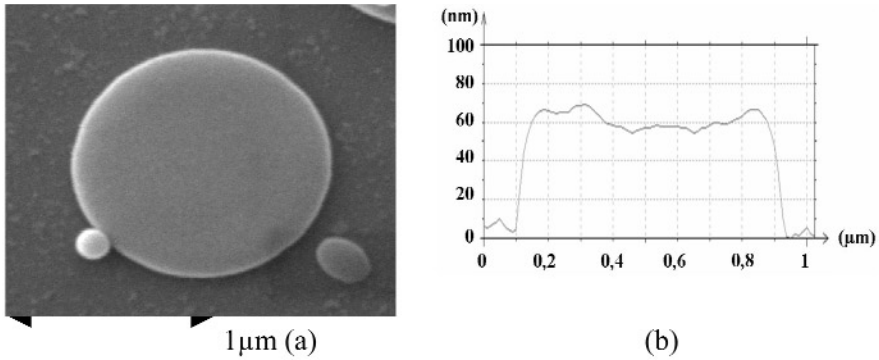

Fig. 5 (a) Zirconia splat resulting from suspension plasma spraying and (b) its profile.

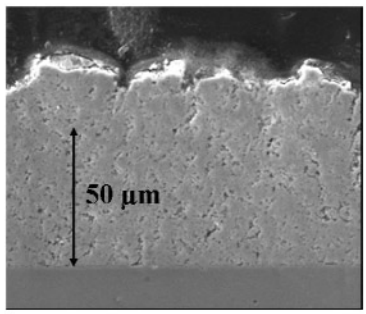

Fig. 6 Stabilized zirconia (13 wt% yttria) coating from suspension plasma spraying [36].

PRODUCTION OF MOLTEN DROPLETS

Plasma torches

The main goal is to adapt the plasma torch velocity as well as the plasma gas specific mass and viscosity (through its temperature and composition) to achieve the desired particle acceleration and velocity. The particle melting is obtained by adapting the plasma-forming gas composition (vol% of hydrogen, nitrogen, helium) to the particle material and velocity. For plasma temperature, two types of level can be achieved [37]: with radio frequency (rf) torches as well as with vortex-type dc torches $T < 10\,000$ K, while with conventional dc torches $T < 13\,000$ K. For an Ar–H_2 mixture and a PTF4-type torch, the gas velocity [37] is given by $v = A \times I^{0.48} \times d^{-2} \times \dot{m}_g^{0.2}$ with I = arc current, d = nozzle internal diameter, and $\dot{m}_g$ = plasma-forming gas mass flow rate.

The gas temperature does not vary much (1000–2000 K) even when the gas enthalpy h is doubled, for example, by increasing the arc current ($h = \rho_{th} \times V \times I\dot{m}_g$) where ρ_{th} is the torch thermal efficiency and V the torch voltage. This is due to the ionization effect: when ionization starts, the slope of the theoretical enthalpy curve is very high and ionization acts as a sort of inertia wheel. The enthalpy, for a given arc current, varies drastically with the plasma-forming gas composition and mass flow rate, parameters which act at the velocity through the coefficient A and $\dot{m}_g$. Thus, as a general rule, a strong increase of h results in a strong rise of v, while the gas temperature is almost constant [39]. The length and diameter of the plasma jet strongly depend on the torch working parameters. With dc torches, typical nozzle inner diameters (i.d.s) are between 6–8 mm for conventional torches, 8–10 mm for high-power vortex dc torches, and 35–50 mm for rf torches. Thus, with dc torches, subsonic gas velocities between 1000–2300 m/s can be achieved, while with rf torches, velocities are below 100 m/s. Rf torches where zirconia particles fully melted can reach 700 m/s have been recently developed. They consist of an rf torch [40] followed by a de Laval nozzle. Particles are injected in the high-pressure (p = 35 kPa)

chamber upstream of the nozzle and accelerated in the expanding plasma (p = 7 kPa). An advantage of the rf torches against the dc ones is also their ability to use shielding oxidizing gases which can reduce the decomposition of oxides. One of the problems of the dc plasma torch is the engulfment process induced by the high-velocity gas exiting in the torch surrounding atmosphere [5]. It can be improved by using de Laval nozzles [41], and works are in progress in this field. The second problem is the arc root fluctuations [42] in the 5000 Hz range, which are mandatory for the anode to survive, but result in voltage fluctuations and plasma jets continuously varying in length and diameter. New torches with segmented anodes allow the arc to be lengthened and, thus, increase its voltage remedy, at least partially, to this problem: the voltage fluctuation amplitude becomes smaller compared to the torch mean voltage. Owing to the engulfment process and the arc root fluctuations, the conventional turbulence models such as low Reynolds K-ε, underestimate the surrounding gas entrainment by the torch [5].

Particle injection

For dc torches, it is a key parameter which consists in adapting the particle mean momentum through the carrier gas flow rate, to that of the plasma jet [43,44]. For rf torches with axial injection, the problem is more the position of the probe and the divergence of the particle jet outside the injector.

Conventional plasma spraying

It is impossible to adjust the carrier gas flow rate to the arc root fluctuations, and, thus, the particle trajectories will be continuously fluctuating around a mean value. The particle velocity (see Fig. 7) and temperature at impact will thus be time-dependent, the agreement between prediction and measurements being good [45].

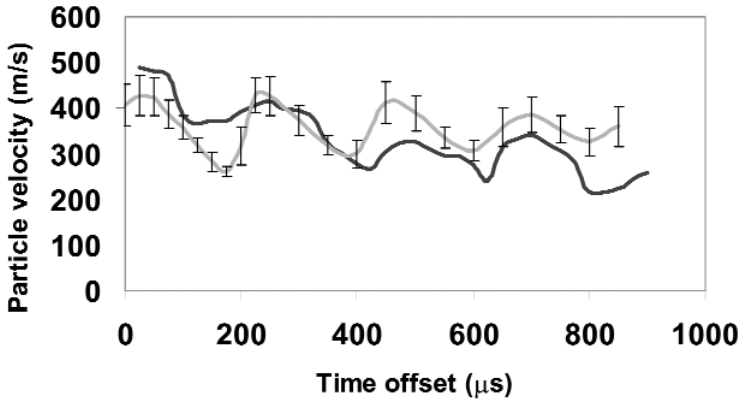

Fig. 7 Time evolution of the calculated and measured velocity of alumina particles ($\bar{d}$ = 30 ± 5 μm) in dc plasma jet (I = 550 A, P = 37 kW, Ar/H_2:35/10 slm, swirl flow) external injection (carrier gas: 3 slm Ar), anode i.d. 7 mm.

Another important problem is linked to the particle size distribution. When the mean particle diameter d_p decreases, the carrier gas flow rate has to be increased accordingly. As the injector i.d. is small, it induces a perturbation of the plasma jet [39]. Besides, when the particle diameter is below 20 μm, especially for light ones, their collisions with the injector wall increase as well as the particle jet divergence at the nozzle exit. As a rule of thumb, it is very difficult to spray particles below 5–10 μm.

Suspension plasma spraying

The main idea is to inject big particles (>100–200 μm) of a suspension of nanoparticles. When injecting them in an rf torch, the liquid is fed by a peristaltic pump and then gas-atomized [46]. After evaporating the solvent, fully molten particles (hydroxyapatite, zirconia…) in the tens of μm range are ob-

tained which can be used to achieve either a conventional coating or dense particles. In a dc plasma flow [35,36,47], big drops (~300 μm) of suspension of nanosized particles are mechanically injected, sheared into tiny droplets (0.5–5 μm depending on plasma jet velocity) that evaporate in less than 1 μs. The agglomerates of nanoparticles resulting from the solvent evaporation are melted ($0.1 < d < 1$ μm) and accelerated toward the substrate where they form splats. The process is illustrated in Fig. 8, and typical splats are shown in Fig. 5. Mechanical injection perturbs much less the plasma flow than atomization, and the injected drop size is controllable [47].

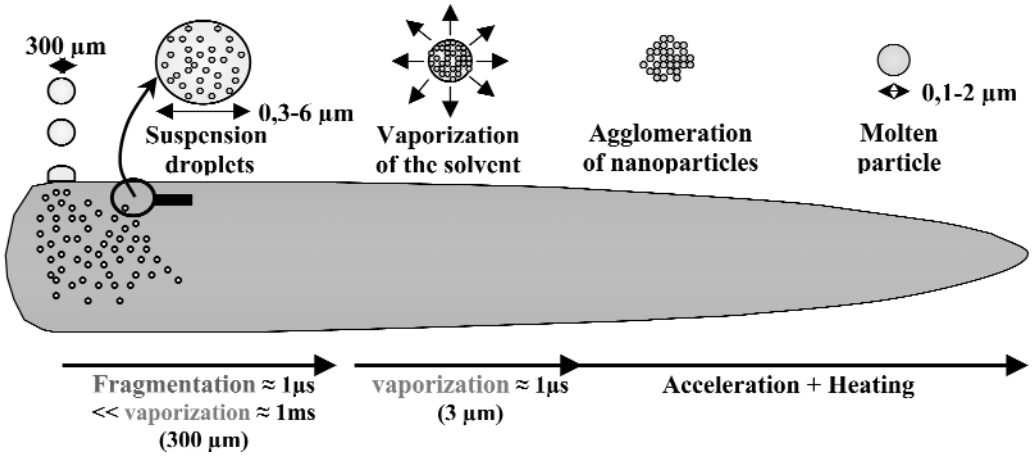

Fig. 8 Mechanism of suspension dc plasma spraying [35].

On-line control

It has been developed for conventional plasma spraying and more generally for thermal spraying [6]. Two types of parameters are controlled: on the one hand, particles in-flight parameters and, on the other hand, substrate and coating temperature evolution. The former are: particle temperature, velocity and heat flux distribution, or only the heat flux distribution closely linked to particle injection. The latter can make use of IR pyrometer or IR thermography camera. It controls the coating adhesion and residual stress distribution. However, at the moment, this on-line control should be called on-line monitoring. It consists mainly in determining a window of good working conditions, based on the sensors used, allowing reproducible and reliable properties of coatings. Nothing has yet been developed for the suspension spraying.

CONCLUSIONS

For conventional coatings, the understanding of plasma–particle interactions has made great strides, and efforts dedicated to the study of splat formation are now in progress. However, for the modeling of the engulfment process in the gas flow, compressive flows, arc root fluctuations, and interface between flattening particles and underlying layers, works are still challenging. Modeling and measurements on splat layering and coating formation have just started. Many works are necessary to understand the links between coating properties (thermomechanical and/or service) and mean coating temperature-time evolution together with the parameters of impacting particles. The latter depend on spraying macroscopic parameters, and databanks have to be systematically established for different substrate-coating couples with specific service conditions. The developed on-line control, or more precisely monitoring, with sensors for particle parameters at impact and coating temperature, have made it possible to reduce the percentage of rejected part and number of quality tests. However, this monitoring will become a control only when the relationships between coating properties and spray parameters exist. Plasma-sprayed or,

more generally, thermal-sprayed nanostructured coatings are still in their infancy, and, for example, for agglomerated nanoparticles the spray conditions are not yet clearly defined even if the coatings exhibit interesting properties. Dc suspension plasma spraying is very promising because it makes it possible to achieve coatings with thickness in the 1 µm to hundreds of µm range, a good deposition efficiency (50 %) and rate (100 nm·m^2/min), a fine structure with a controllable porosity, finely graded structures, and intricated interfaces. However, many works are still necessary.

REFERENCES

1. L. Pawlowski. *The Science and Engineering of Thermal Spray Coatings*, John Wiley, New York (1995).
2. P. Fauchais, A. Vardelle, B. Dussoubs. Review paper, *J. Therm. Spray Technol*. **10**, 44–66 (2001).
3. L. L. Shaw, D. Goberman, R. Ren, M. Gell, S. Jiang, Y. Wang, T. D. Xiao, P. R. Strutt. *Surf. Coat. Technol*. **130**, 1–8 (2000).
4. P. Fauchais, J. F. Coudert, M. Vardelle. *J. High Temp. Mater. Proc*. **6**, 247–265 (2002).
5. G. Mariaux and A. Vardelle. *Int. J. Therm. Sci.* (2003). Accepted for publication.
6. P. Fauchais and M. Vardelle. In *Thermal Spray 2003: Advancing the Science & Applying the Technology*, C. Moreau and B. Marple (Ed.), pp. 1165–1173, ASM Int. Materials Park OH (2003).
7. P. Fauchais, M. Fukumoto, A. Vardelle, M. Vardelle. Review paper, *J. Therm. Spray Technol.* **13**, 337–360 (2003).
8. C. C. Berndt and E. J. Lavernia. *J. Therm. Spray Technol*. **7**, 411–441 (1998).
9. T. Stoltenhoff, H. Kreye, H. J. Richter. *J. Therm. Spray Technol.* **11**, 542–550 (2002).
10. G. Espié, A. Vardelle, J. C. Labbe, P. Fauchais. *Thin Solid Films* (2003). Accepted for publication.
11. S. Q. Armster, J. P. Delplanque, M. Rein, E. J. Lavernia. *Int. Mater. Rev*. **7**, 265–301 (2002).
12. C. Escure, M. Vardelle, P. Fauchais. *Plasma Chem. Plasma Proc*. **23**, 185–222 (2003).
13. J. Cedelle, M. Vardelle, B. Pateyron, P. Fauchais. *J. High Temp. Mater. Proc.* **8**, 397–407 (2004).
14. M. Vardelle, A. Vardelle, P. Fauchais, C. Moreau. *Meas. Sci. Technol.* **5**, 205–213 (1994).
15. S. Fantassi, M. Vardelle, A. Vardelle, P. Fauchais. *J. Therm. Spray Technol*. **2** (4), 379–384 (1993).
16. M. Vardelle, A. Vardelle, A. C. Léger, P. Fauchais, D. Gobin. *J. Therm. Spray Technol*. **4** (1), 50–58 (1994).
17. C. Moreau, P. Cielo, M. Lamontagne. *J. Therm. Spray Technol.* **1** (4), 317–323 (1992).
18. C. Moreau, P. Gougeon, M. Lamontagne. *J. Therm. Spray Technol*. **4** (1), 25–36 (1995).
19. P. Gougeon and C. Moreau. *J. Therm. Spray Technol*. **10** (1), 76–82 (2001).
20. M. Fukumoto, S. Katoh, I. Okane. In *Proc. of the 14th Int. Therm. Spray Conf*., A. Ohmori (Ed.), High Temp Soc. of Japan **1**, 353–359 (1995).
21. N. Z. Mehdizadeh, S. Chandra, J. Mostaghimi. In *Proc. of Int. Therm. Spray Conf., Essen 2002*, E. Lugscheider (Ed.), DVS Düsseldorf, 830–837 (2002).
22. S. Pasandideh-Fard, V. Pershin, S. Chandra, J. Mostaghimi. *J. Therm. Spray Technol*. **11**, 206–217 (2002).
23. A. Vardelle, M. Vardelle, P. Fauchais, D. Gobin. *NATO Ser. E, Appl. Sci*. **282**, 95–121 (1995).
24. S. Sampath and H. Herman. *J. Therm. Spray Technol*. **5**, 445–456 (1996).
25. A. Vardelle, C. Moreau, P. Fauchais. *MRS Bull.* 32–37 (2000).
26. A. Vardelle, M. Vardelle, H. Zang, N. J. Themlis, K. Gross. *J. Therm. Spray Technol*. **11**, 244–252 (2002).
27. S. Kuroda, T. Dendo, S. Kitahara. *J. Therm. Spray Technol*. **4**, 75–84 (1995).
28. T. W. Clyne and S. C. Gill. *J. Therm. Spray Technol*. **5**, 401–418 (1996).

29. R. Ghafouri-Azar, J. Mostaghimi, S. Chandra, M. Charnchi. *J. Therm. Spray Technol*. **12**, 53–69 (2003).
30. P. Fauchais, M. Vardelle, A. Vardelle, L. Bianchi, A. C. Leger. *Plasma Chem. Plasma Proc*. **16**, 99S–126S (1996).
31. S. Lima, A. Kucak, C. C. Berndt. *Mater. Sci. Eng*. **A327**, 224–232 (2002).
32. M. Gell, E. M. Jordan, Y. H. Soha, D. Goberman, L. Shaw, T. D. Xiao. *Surf. Coat. Technol*. **146–147**, 48–54 (2001).
33. Nanosteel Co., 485 North Keller Rd., Suite 100, Maitland, FL 32751, USA.
34. J. Karthikeyan, C. C. Berndt, J. Tikkaren, J. Y. Wang, A. H. King, H. Herman. *Nanostruct. Mater*. **8**, 61–74 (1997).
35. J. Fazilleau, C. Delbos, M. Violier, J. F. Coudert, P. Fauchais, L. Bianchi, K. Wittmann-Ténèze. In *Thermal Spray 2003: Advancing the Science & Applying the Technology*, C. Moreau and B. Marple (Eds.), pp. 889–893, ASM Int. Materials Park OH (2003).
36. C. Delbos, J. Fazilleau, J. F. Coudert, P. Fauchais, L. Bianchi, K. Wittmann-Ténèze. In *Thermal Spray 2003: Advancing the Science & Applying the Technology,* C. Moreau and B. Marple (Eds.), pp. 661–669, ASM Int. Materials Park OH (2003).
37. P. Fauchais and A. Vardelle. Review paper. *Int. J. Therm. Sci*. **39**, 852–870 (2000).
38. J. F. Coudert, M. P. Planche, P. Fauchais. *Plasma Chem. Plasma Proc*. **15**, 47–70 (1985).
39. P. Fauchais, A. Vardelle, N. Themelis. *Plasma Chem. Plasma Proc*. **18**, 551–574 (1998).
40. G. Renouard-Vallet, F. Guitzhofer, M. Boulos, P. Fauchais, M. Vardelle, L. Bianchi. In *Thermal Spray 2003: Advancing the Science & Applying the Technology*, C. Moreau and B. Marple (Eds.), pp. 195–202, ASM Int. Materials Park, OH (2003).
41. G. Schiller, R. Henne, V. Borck. *J. Therm. Spray Technol*. **4**, 185–194 (1995).
42. J. Heberlein. In *Heat and Mass Transfer under Plasma Condition*, Ann. N.Y. Acad. Sci. **891**, 14–27 (1999).
43. M. Vardelle and P. Fauchais. *Pure Appl. Chem*. **71**, 1909–1918 (1999).
44. M. Vardelle, A. Vardelle, P. Fauchais, K. I. Li, B. Dussoubs, N. J. Themlis. *J. Therm. Spray Technol*. **10**, 267–286 (2001).
45. J. F. Bisson, B. Gauthier, C. Moreau. *J. Therm. Spray Technol*. **12**, 38–43 (2003).
46. E. Bouyer, F. Guitzhofer, M. I. Boulos. *IEEE Trans. Mater. Sci*. **25**, 1066–1072 (1997).
47. K. Wittmann, J. Fazilleau, J. F. Coudert, P. Fauchais, F. Blein. In *Proc. of ITSC 2002*, E. Lugsheider (Ed.), DVS, Düsseldorf, 519–522 (2002).